Mode structure and attenuation characteristics of hollow parabolic waveguides

Rodrigo J. Noriega-Manez and Julio C. Gutiérrez-Vega*

Photonics and Mathematical Optics Group, Tecnológico de Monterrey, Monterrey, Mexico 64849
**Corresponding author: juliocesar@itesm.mx*

Received March 27, 2007; accepted June 6, 2007;
posted June 21, 2007 (Doc. ID 81559); published August 20, 2007

The mode structure and attenuation constants in parabolic hollow waveguides with arbitrary parabolic domains are investigated based on the exact vector field expressions and characteristic equations. Normalized attenuation charts are provided for a variety of mode numbers, parities, and polarizations. The analysis is not restricted to parabolic waveguides with a symmetric cross section. © 2007 Optical Society of America

OCIS codes: 230.7370, 260.2110, 260.1960, 350.5500.

1. INTRODUCTION

It is well known that the only types of waveguides for which the scalar wave equation may be separated are those whose cross sections are either rectangular, circular, elliptical, or parabolic [1,2]. The first three have been well investigated, but the fourth has received little attention. The formal solution for the propagating electromagnetic modes in parabolic guides was presented first by Spence and Wells in 1942 [3], and later by Morse and Feshbach [4] in 1952. Because of the difficulties in accurately evaluating the parabolic cylinder functions, these seminal works were focused to study only theoretical aspects. More recently, Kenney and Overfelt [5] provided an efficient and accurate numerical method to calculate the eigenvalues of the transverse magnetic (TM) and transverse electric (TE) modes in parabolic pipes and applied it to determine the power handling efficiency factors for several lower order modes. It should be mentioned that the analysis in [3–5] was restricted to parabolic pipes with symmetrical cross sections.

In recent years the study of field propagation in parabolic geometries has witnessed a revival of research interest. In particular, the existence of linearly polarized parabolic optical beams, which constitute the fourth complete family of nondiffracting optical beams, was theoretically demonstrated [6], and experimentally observed [7] in free space. Even more recently, we reported closed-form expressions for the scalar and vector paraxial propagation of the parabolic-Gaussian beams traveling in both vacuum and general ABCD systems [8–12].

In this paper, we extend our previous works to the case of electromagnetic propagation in parabolic waveguides, and present a study of the mode structure and attenuation characteristics of hollow parabolic waveguides with arbitrary parabolic domains. We apply the first-order perturbation theory to determine the exact formulas for the attenuation constants due to conductor losses for TM and TE modes starting from the ideal propagating modes in perfect-conducting pipes. We numerically evaluate the attenuation constants and provide attenuation charts for a continuous variation of the cross parabolic domain. Knowledge of the losses is necessary for designers who need to estimate the practical utility of parabolic structures. This work extends and consolidates previous analysis on propagating modes and attenuation constants in parabolic waveguides [3–5].

2. MODE STRUCTURE

Let us consider a parabolic cylindrical waveguide of uniform cross section completely filled by a homogeneous lossless dielectric medium with permittivity ϵ and permeability μ. The geometry of the pipe is shown in Fig. 1, where the parabolic coordinates and their ranges are defined. The surface of the waveguide is formed by the intersection of the two parabolic surfaces $\xi=\xi_0$ (left wall) and $\eta=\eta_0$ (right wall). Throughout the paper we assume the usual $\zeta(z,t)=\exp[i\omega t-(\alpha+i\beta)z]$ dependence for traveling waves in the positive z direction, where α and β are real and positive constants.

We first describe the mode structure in parabolic pipes to establish notation and to provide a reference point for necessary formulas. The traveling modes can be written in closed form in terms of the even $\mathrm{P}_e(\nu;a)$ and odd $\mathrm{P}_o(\nu;a)$ solutions of the parabolic cylinder equation:

$$\left[\frac{\mathrm{d}^2}{\mathrm{d}\nu^2}+\frac{\nu^2}{4}-a\right]\begin{Bmatrix}\mathrm{P}_e(\nu;a)\\ \mathrm{P}_o(\nu;a)\end{Bmatrix}=0, \tag{1}$$

where $a\in(-\infty,\infty)$ is the real and continuous eigenvalue of the differential equation [13]. In particular, the longitudinal and transverse field components of the even TM modes ($H_z=0$) are written as follows:

$$E_z=\mathrm{P}_e(\sqrt{2\kappa}\xi;a)\mathrm{P}_e(\sqrt{2\kappa}\eta;-a)\zeta(z,t), \tag{2a}$$

$$\mathbf{E}_t=-\frac{i\beta}{\kappa^2}\nabla_t E_z, \tag{2b}$$

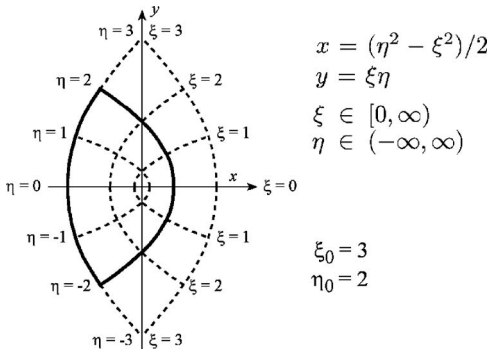

Fig. 1. Geometry of the parabolic waveguide and the definition of the parabolic coordinates.

$$\mathbf{H}_t = \frac{i\omega\epsilon}{\kappa^2}\hat{\mathbf{z}} \times \nabla_t E_z, \tag{2c}$$

where $\kappa=(\omega^2\mu\epsilon-\beta^2)^{1/2}$ is the transverse wavenumber of the mode, ∇_t is the transverse gradient operator expressed in parabolic coordinates, and the longitudinal field is restricted to satisfy the boundary conditions

$$\mathrm{P}_e(\sqrt{2\kappa}\xi_0;a)=0, \quad \text{TM modes}, \tag{3a}$$

$$\mathrm{P}_e(\sqrt{2\kappa}\eta_0;-a)=0, \quad \text{TM modes}. \tag{3b}$$

Odd parity TM modes can be obtained by writing the odd functions $\mathrm{P}_o(\nu;a)$ instead of the even ones in Eqs. (2) and (3).

Equations (2) and (3) define the electromagnetic modes with TM polarization. TE modes ($E_z=0$) can be readily obtained from Eq. (2) by applying the duality property (i.e., replacing $\mathbf{E}$ with $(\mu/\epsilon)^{1/2}\mathbf{H}$ and $(\mu/\epsilon)^{1/2}\mathbf{H}$ with $-\mathbf{E}$) subject to the boundary conditions

$$\mathrm{P}'_e(\sqrt{2\kappa}\xi_0;a)=0, \quad \text{TE modes}, \tag{4a}$$

$$\mathrm{P}'_e(\sqrt{2\kappa}\eta_0;-a)=0, \quad \text{TE modes}, \tag{4b}$$

where the prime denotes the derivative of the function $\mathrm{P}_e(\nu;a)$ with respect to its argument.

For a given value of ξ_0, Eq. (3a) defines a family of curves relating κ and a (plotting κ as a function of a). The curve closest to the a axis may be labeled $m=1$, the next $m=2$, and so on. Equation (3b) produces another set of curves on the (a,κ) plane, the lowest of which may be labeled $n=1$, the next $n=2$, etc. Every point wherever these two families of curves cross defines an allowed value of a (called $a_{m,n}$), and an allowed value of κ (called $\kappa_{m,n}$). The pair $(a_{m,n},\kappa_{m,n})$ defines the corresponding eigenmode ${}_e\mathrm{TM}_{m,n}$. Proceeding in the same manner, the intersections of the families of curves generated by Eqs. (3a) and (3b), using the odd functions P_o, generate the odd modes ${}_o\mathrm{TM}_{m,n}$ with $m=1,2,\ldots$ and $n=1,2,\ldots$. By this means we obtain all the allowed even and odd TM modes and their eigenvalues of the guide. For a given mode (m,n) with transverse wavenumber $\kappa_{m,n}$, its cutoff frequency $\omega^c_{m,n}$ is determined under the condition $\beta=0$, which leads to

$$\omega^c_{m,n}=\frac{\kappa_{m,n}}{\sqrt{\mu\epsilon}}. \tag{5}$$

At any z plane the transverse distribution of the longitudinal fields is proportional to the scalar function

$$\psi_{m,n}=\mathrm{P}_e(\sqrt{2\kappa}\xi;a)\mathrm{P}_e(\sqrt{2\kappa}\eta;-a). \tag{6}$$

Several shapes of (a) TM and (b) TE modes are depicted in Fig. 2 for a variety of mode numbers and boundary ratios $s=\xi_0/\eta_0$. Note that the fields in Fig. 2 exhibit well defined parabolic nodal lines. The mode numbers m and n correspond to the number of nodal lines along curves with η

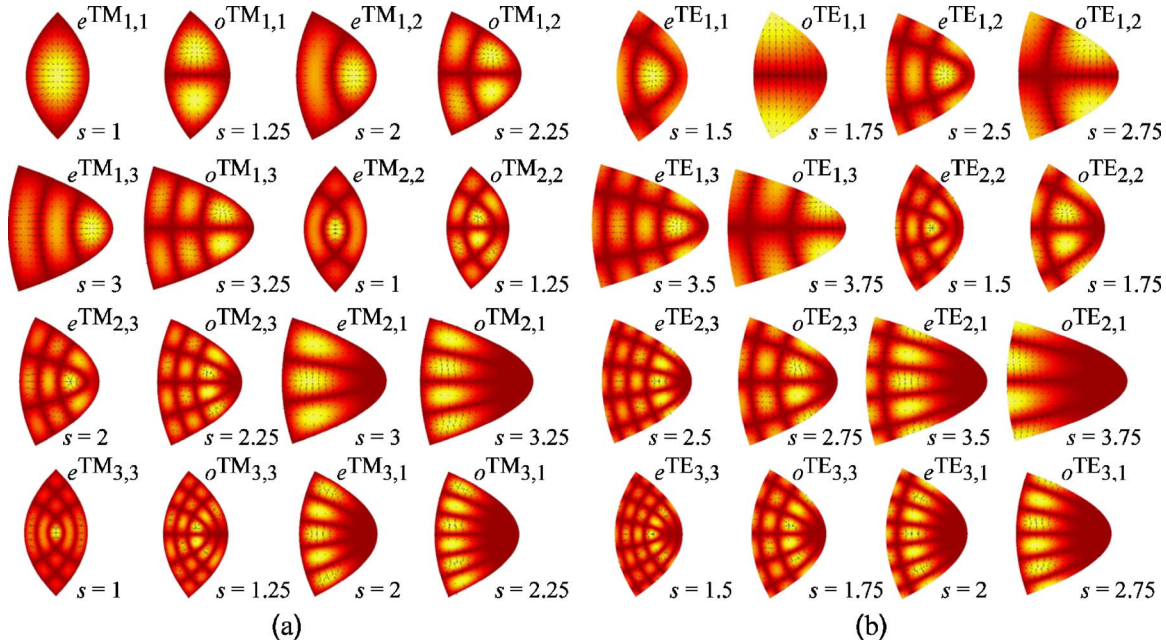

Fig. 2. (Color online) Absolute value of (a) E_z in TM modes, and (b) H_z in TE modes, for a variety of mode numbers, parities, and boundary ratios $s=\xi_0/\eta_0$.

and ξ constant, respectively, taking into account the symmetry line $y=0$ for odd modes, and the boundary nodal line for TM modes. The patterns are symmetrical about the x-axis, i.e., ${}_{e,o}\psi(x,-y;a)=\pm{}_{e,o}\psi(x,y;a)$, where plus and minus signs correspond to the even and odd modes, respectively. For $\xi_0>\eta_0$ the curvature of the right parabolic wall is larger than the curvature of the left one (see Fig. 1) with the consequence that all eigenvalues $a_{m,n}$ are positive. The modes for $\eta_0<\xi_0$ correspond to eigenvalues $a_{m,n}<0$, and follow a similar behavior since fields satisfy the symmetry relation ${}_{e,o}\psi(x,y;-a)={}_{e,o}\psi(-x,y;a)$. The symmetrical mode for $a=0$ can be present only when the pipe is also symmetrical about the y-axis, i.e., $\xi_0=\eta_0$.

There are some mathematical properties of the transverse solutions to be discussed here. The solutions $\psi_{m,n}$ are orthogonal; this means that $\iint\psi_{m,n}\psi_{p,q}\,dS=\delta_{m,p}\delta_{n,q}$, where $\delta_{m,p}$ is the Kronecker delta and the integration is carried out over the transverse cross section of the guide. A general field propagating through the guide is found by superposing the infinite number of allowed TM and TE modes. Because of the linearity and the one-to-one mapping of the gradient operator, the properties of linear independence, orthogonality, and completeness exhibited by the family of scalar solutions $\psi_{m,n}$ are transferred to the corresponding families of vector fields $\mathbf{E}_t$, with the consequence that the TM and TE modes form a complete and orthogonal basis that is useful to describe the general electromagnetic propagation in parabolic waveguides.

We have applied the analytic continuation method described in Ref. [5] for evaluating the even and odd parabolic functions and their derivatives. Our routines have also been used to reproduce the sequence of eigenvalues in a parabolic waveguide, showing excellent agreement with the values reported in the literature [3–5].

3. LOSSES DUE TO CONDUCTING WALLS

According to the first-order perturbation method [1], the attenuation constant α [Np/m] for a given propagating mode (m,n) is given by

$$\alpha=\frac{P_L}{2P_T}=\frac{1}{2}\frac{\oint_l Z_{\text{wall}}|\mathbf{H}_{\tan}|^2 dl}{\int_S Z_{\text{wave}}|\mathbf{H}_t|^2 dS}, \tag{7}$$

where P_L is the per-unit length power loss, and P_T is the power flowing through the waveguide, $Z_{\text{wall}}=\sqrt{\omega\mu_w/2\sigma}$ is the constant surface impedance, μ_w is the permeability of the conducting walls, σ is the finite conductivity of the walls (assumed independent of the frequency), $\mathbf{H}_{\tan}$ is the tangential component of the magnetic field at the walls assuming the lossless condition, l is the contour enclosing the cross-section, S is the cross-section area, $Z_{\text{wave}}=\beta/\omega\epsilon$ for TM modes, and $Z_{\text{wave}}=\omega\mu/\beta$ for TE modes.

By replacing the field expressions Eq. (2) into Eq. (7) we find the following general expressions for the attenuation constants:

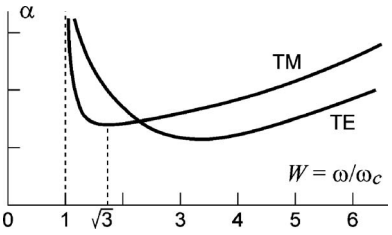

Fig. 3. General behavior of the attenuation constants as a function of the normalized frequency W for both TM and TE modes.

$$\alpha_{TM}\sqrt{\frac{2\sigma Z\mu}{\mu_w}}=f_{m,n}(\xi_0,\eta_0)\sqrt{\frac{W^3}{W^2-1}}, \tag{8}$$

$$\alpha_{TE}\sqrt{\frac{2\sigma Z\mu}{\mu_w}}=g_{m,n}(\xi_0,\eta_0)\sqrt{\frac{W^2-1}{W}}+\frac{h_{m,n}(\xi_0,\eta_0)}{\sqrt{W^3-W}}, \tag{9}$$

where $Z=\sqrt{\mu/\varepsilon}$ is the intrinsic impedance of the dielectric medium, W is the normalized angular frequency

$$W=\frac{\omega}{\omega_c}=\frac{\omega\sqrt{\mu\epsilon}}{\kappa}\geqslant 1, \tag{10}$$

and the factors f, g, and h depend exclusively on the physical dimensions of the guide upon

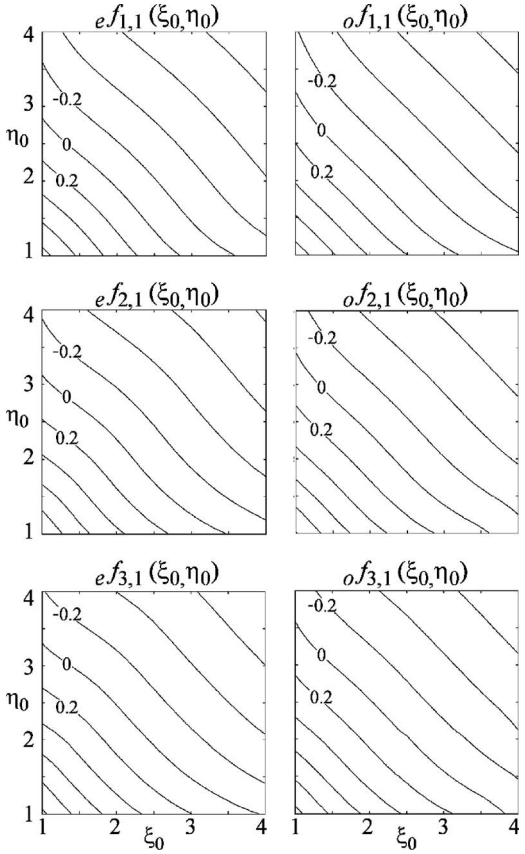

Fig. 4. Contour plots of $\log(f_{m,n})$ on the plane (ξ_0,η_0) for the lowest order even and odd modes. Labels corresponding to $\log(f_{m,n})=\{-0.2,0,0.2\}$ are included in the plots; remaining labels have been omitted for clarity. For all plots, the separation between consecutive contour lines is 0.2, and $1\leqslant\xi_0\leqslant 4$ and $1\leqslant\eta_0\leqslant 4$.

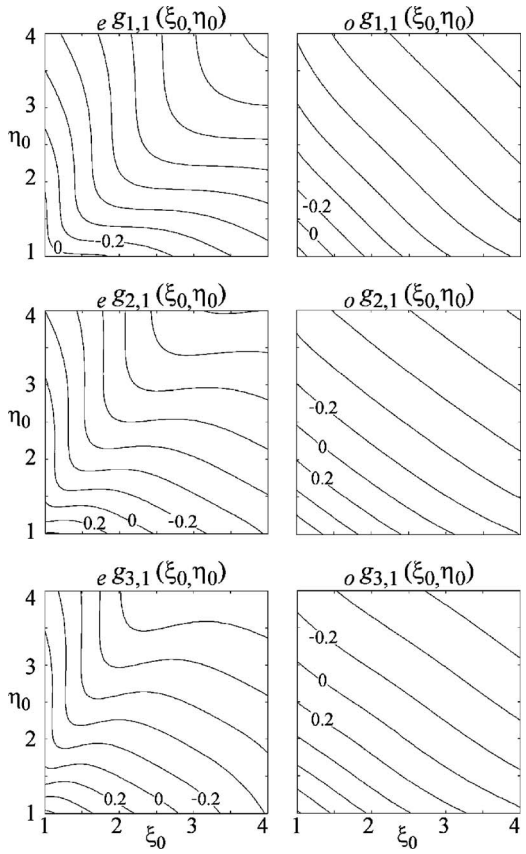

Fig. 5. Contour plots of $\log(g_{m,n})$ on the plane (ξ_0, η_0) for the lowest order even and odd modes. Labels corresponding to $\log(g_{m,n}) = \{-0.2, 0, 0.2\}$ are included in the plots; remaining labels have been omitted for clarity. For all plots, the separation between consecutive contour lines is 0.2, and $1 \leqslant \xi_0 \leqslant 4$ and $1 \leqslant \eta_0 \leqslant 4$.

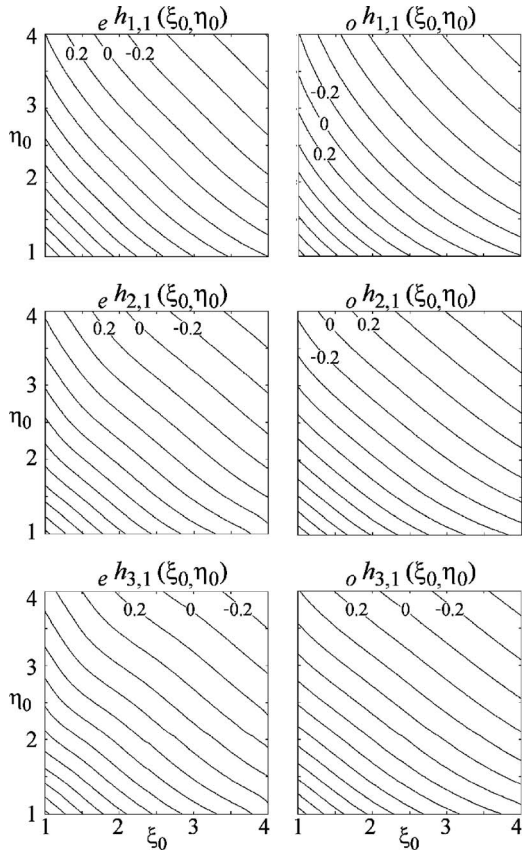

Fig. 6. Contour plots of $\log(h_{m,n})$ on the plane (ξ_0, η_0) for the lowest order even and odd modes. Labels corresponding to $\log(h_{m,n}) = \{-0.2, 0, 0.2\}$ are included in the plots; remaining labels have been omitted for clarity. For all plots, the separation between consecutive contour lines is 0.2, and $1 \leqslant \xi_0 \leqslant 4$ and $1 \leqslant \eta_0 \leqslant 4$.

$$f_{m,n}(\xi_0, \eta_0) = \sqrt{\kappa_{m,n}}\left(\frac{A+B}{F}\right), \tag{11}$$

$$g_{m,n}(\xi_0, \eta_0) = \sqrt{\kappa_{m,n}}\left(\frac{K+L}{F}\right), \tag{12}$$

$$h_{m,n}(\xi_0, \eta_0) = \sqrt{\kappa_{m,n}}\kappa_{m,n}^2\left(\frac{I+J}{F}\right), \tag{13}$$

with

$$F = \int_0^{\xi_0}\int_0^{\eta_0}(U^2V'^2 + U'^2V^2)\mathrm{d}\xi\mathrm{d}\eta, \tag{14a}$$

$$A = V'^2(\eta_0)\int_0^{\xi_0} U^2(\xi^2 + \eta_0^2)^{-1/2}\mathrm{d}\xi, \tag{14b}$$

$$B = U'^2(\xi_0)\int_0^{\eta_0} V^2(\xi_0^2 + \eta^2)^{-1/2}\mathrm{d}\eta, \tag{14c}$$

$$I = V^2(\eta_0)\int_0^{\xi_0} U^2(\xi^2 + \eta_0^2)^{1/2}\mathrm{d}\xi, \tag{14d}$$

$$J = U^2(\xi_0)\int_0^{\eta_0} V^2(\xi_0^2 + \eta^2)^{1/2}\mathrm{d}\eta, \tag{14e}$$

$$K = V^2(\eta_0)\int_0^{\xi_0} U'^2(\xi^2 + \eta_0^2)^{-1/2}\mathrm{d}\xi, \tag{14f}$$

$$L = U^2(\xi_0)\int_0^{\eta_0} V'^2(\xi_0^2 + \eta^2)^{-1/2}\mathrm{d}\eta, \tag{14g}$$

where the short notations $U(\xi) \equiv \mathrm{P}_e(\sqrt{2\kappa_{m,n}}\xi; a_{m,n})$ and $V(\eta) \equiv \mathrm{P}_e(\sqrt{2\kappa_{m,n}}\eta; -a_{m,n})$ have been adopted for the even modes, and $U(\xi) \equiv \mathrm{P}_o(\sqrt{2\kappa_{m,n}}\xi; a_{m,n})$ and $V(\eta) \equiv \mathrm{P}_o(\sqrt{2\kappa_{m,n}}\eta; -a_{m,n})$ for the odd modes.

The expressions in Eqs. (8) and (9) explicitly exhibit the frequency dependence of the attenuation constants of the parabolic guides. Given the dimensions of the guide, the general behavior of the attenuation constants as a function of the frequency is shown in Fig. 3. At high frequencies the attenuation increases as $\omega^{1/2}$ for both TM and TE modes. The first-order perturbation method employed in obtaining Eq. (7) breaks down very close to the cutoff. Evidence for this is the physically impossible, infinite value of α_{TM} and α_{TE} at $W=1$.

Table 1. Values of the Coefficients c_1, c_2, and c_3 for the Different Values of m and n

Mode	$c_{1,m,n}$	$c_{2,m,n}$	$c_{3,m,n}$
$e_{1,1}$	7.437	1.383	158.35
$o_{1,1}$	8.161	3.039	30.704
$e_{2,1}$	9.569	2.565	286.73
$o_{2,1}$	10.16	6.022	138.93
e_{31}	10.948	4.423	453.83
$o_{3,1}$	11.587	10.531	319.21

For any combination of ξ_0 and η_0 there is a frequency value where the modes have the lowest attenuation. The value of $W_{\min}$ is determined by differentiating Eqs. (8) and (9) with respect to W, and equating them to zero. For TM modes, we find that the minimum attenuation always occurs at $W_{\min}^{TM}=\omega_{\min}/\omega_c=\sqrt{3}$ regardless of the mode numbers (m,n) and the boundary walls (ξ_0,η_0). For TE modes, the frequency dependence of α_{TE} cannot be extracted as a single factor in Eq. (9), therefore, the frequency $W_{\min}^{TE}$ at which minimum attenuation occurs depends on the cross-sectional geometry, namely,

$$W_{\min}^{TE}(\xi_0,\eta_0)=\sqrt{\frac{3h}{2g}+\sqrt{\left(\frac{3h}{2g}\right)^2-\frac{h}{g}+1}}, \tag{15}$$

where g and h are given by Eqs. (12) and (13).

From Eqs. (8) and (9) it is clear that the effect of the guide geometry on the attenuation constants is determined by the behavior of the functions $f_{m,n}(\xi_0,\eta_0)$, $g_{m,n}(\xi_0,\eta_0)$, and $h_{m,n}(\xi_0,\eta_0)$. Rather than plotting α_{TM} and α_{TE} as functions of the frequency for some combinations of ξ_0 and η_0, in Figs. 4–6 we plot the functions f, g, and h on the plane (ξ_0,η_0) for the lowest order even and odd modes, respectively. This representation clearly reveals the dependence of the attenuation constants over a continuous variation of the guide geometry, and provides more useful charts to calculate the attenuation constants for the parabolic guides. In the computation of the functions f, g, and h, we have taken advantage of the separability of F [Eq. (14a)] to split it into single integrals, and we have applied a 300-point Gauss–Legendre quadrature to evaluate all integrals in Eqs. (14a)–(14g).

The symmetric waveguide when $\xi_0=\eta_0$ is of special interest. In this case, it is possible to demonstrate that $f_{m,n}(\xi_0,\xi_0)$, $g_{m,n}(\xi_0,\xi_0)$, and $h_{m,n}(\xi_0,\xi_0)$ reduce to the following remarkable simple expressions:

$$f_{m,n}(\xi_0,\xi_0)=\frac{c_{1,m,n}}{\xi_0^3}, \tag{16}$$

$$g_{m,n}(\xi_0,\xi_0)=\frac{c_{2,m,n}}{\xi_0^3}, \tag{17}$$

$$h_{m,n}(\xi_0,\xi_0)=\frac{c_{3,m,n}}{\xi_0^5}, \tag{18}$$

where the coefficients $c_{1,m,n}$, $c_{2,m,n}$, and $c_{3,m,n}$, depend on the indices (m,n) and the parity of the mode, but are independent of the boundary ξ_0. The coefficients c_1, c_2, and c_3 can be easily obtained by evaluating the functions f, g, and h at the point $(\xi_0,\eta_0)=(1,1)$ in Figs. 4–6, and the results are given in Table 1.

4. CONCLUSIONS

The first-order perturbation method has been used to calculate the attenuation constants due to conductor losses in parabolic waveguides with arbitrary parabolic regions. In the course of obtaining these expressions, we included a description of the full electromagnetic propagation in conductive parabolic waveguides. A suitable rearrangement of the expressions (8) and (9) makes it possible to present useful charts to find α_{TM} and α_{TE} (a) for a continuous combination of boundaries ξ_0 and η_0, and (b) in function of the normalized frequency W. For both TM and TE polarizations, it was possible to explicitly find the frequencies for which a minimum attenuation occurs. The expressions for the attenuation constants Eqs. (8) and (9) resemble those obtained by Gutiérrez-Vega *et al.* [14] for the pipe of the confocal annular elliptical cross section. Both expressions have the same frequency dependence, confirming the fact that the attenuation behavior of the electromagnetic waves is the same for all cylindrical pipes whose cross sections are defined by coordinates that separate the scalar wave equation.

ACKNOWLEDGMENTS

This research was partially supported by Consejo Nacional de Ciencia y Tecnología from Mexico grant 42808, and by the Tecnológico de Monterrey Research Chair in Optics grant CAT-007.

REFERENCES

1. G. F. Miner, *Lines and Electromagnetic Fields for Engineers* (Oxford U. Press, 1996).
2. C. Someda, *Electromagnetic Waves* (Chapman & Hill, 1988).
3. R. D. Spence and C. P. Wells, "The propagation of electromagnetic waves in parabolic pipes," Phys. Rev. **62**, 58–62 (1942).
4. P. Morse and H. Feshbach, *Methods of Theoretical Physics* (McGraw-Hill, 1953), Vol. II.
5. C. S. Kenney and P. L. Overfelt, "A simple approach to mode analysis for parabolic waveguides," IEEE Trans. Microwave Theory Tech. **39**, 405–412 (1991).
6. M. A. Bandres, J. C. Gutiérrez-Vega, and S. Chávez-Cerda, "Parabolic nondiffracting optical wave fields," Opt. Lett. **29**, 44–46 (2004).
7. C. López-Mariscal, M. A. Bandres, S. Chávez-Cerda, and J. C. Gutiérrez-Vega, "Observation of parabolic nondiffracting wave fields," Opt. Express **13**, 2364–2369 (2005).
8. J. C. Gutiérrez-Vega and M. A. Bandres, "Helmholtz–Gauss waves," J. Opt. Soc. Am. A **22**, 289–298 (2005).
9. M. A. Bandres and J. C. Gutiérrez-Vega, "Vector Helmholtz–Gauss and vector Laplace–Gauss beams," Opt. Lett. **30**, 2155–2157 (2005).
10. C. López-Mariscal, M. A. Bandres, and J. C. Gutiérrez-Vega, "Observation of the experimental propagation properties of Helmholtz–Gauss beams," Opt. Eng. (Bellingham) **45**, 068001 (2006).
11. M. Guizar-Sicairos and J. C. Gutiérrez-Vega, "Generalized

Helmholtz–Gauss beam and its transformation by paraxial optical systems," Opt. Lett. **31**, 2912–2914 (2006).
12. R. I. Hernandez-Aranda, Julio C. Gutiérrez-Vega, M. Guizar-Sicairos, and M. A. Bandres, "Propagation of generalized vector Helmholtz–Gauss beams through paraxial optical systems," Opt. Express **14**, 8974–8988 (2006).
13. M. Abramowitz and I. Stegun, *Handbook of Mathematical Functions* (Dover, 1964).
14. Julio C. Gutiérrez-Vega, R. M. Rodríguez-Dagnino, and S. Chávez-Cerda, "Attenuation characteristics in confocal annular elliptic waveguides and resonators," IEEE Trans. Microwave Theory Tech. **50**, 1095–1100 (2002).